

# Vision-only UAV State Estimation for Fast Flights Without External Localization Systems: A2RL Drone Racing Finalist Approach

Filip Novák\*, Matěj Petrlík, Matej Novosad, Parakh M. Gupta, Robert Pěnička, and Martin Saska

**Abstract**—Fast flights with aggressive maneuvers in cluttered GNSS-denied environments require fast, reliable, and accurate UAV state estimation. In this paper, we present an approach for onboard state estimation of a high-speed UAV using a monocular RGB camera and an IMU. Our approach fuses data from Visual-Inertial Odometry (VIO), an onboard landmark-based camera measurement system, and an IMU to produce an accurate state estimate. Using onboard measurement data, we estimate and compensate for VIO drift through a novel mathematical drift model. State-of-the-art approaches often rely on more complex hardware (e.g., stereo cameras or rangefinders) and use uncorrected drifting VIO velocities, orientation, and angular rates, leading to errors during fast maneuvers. In contrast, our method corrects all VIO states (position, orientation, linear and angular velocity), resulting in accurate state estimation even during rapid and dynamic motion. Our approach was thoroughly validated through 1600 simulations and numerous real-world experiments. Furthermore, we applied the proposed method in the A2RL Drone Racing Challenge 2025, where our team advanced to the final four out of 210 teams and earned a medal.

**Index Terms**—Localization, Sensor Fusion, Visual-Inertial SLAM, UAV, Drone Racing

## SUPPLEMENTARY MATERIALS

**Video:** <https://youtu.be/6mLJ1Dx3jNE>

## I. INTRODUCTION

**A**GILE lightweight drones have gained significant attention in recent years, due to their potential ability to fly fast even in a highly cluttered environment. These capabilities make them well-suited for inspection tasks [1], search and rescue operations [2], or security and surveillance missions [3]. Autonomous Unmanned Aerial Vehicles (UAVs) typically operate at low speeds near hover, ensuring adequate time for their sensing systems to collect data to estimate the robot's state within the environment, which is not efficient for the applications mentioned above. Pushing autonomous UAVs towards aggressive maneuvers at high speeds with acceleration up to 7 g in cluttered Global Navigation Satellite System (GNSS)-denied environments, which is tackled in this paper, places significant demands on UAV state estimation, especially when UAV payload capacity for

All authors are with Department of Cybernetics, Faculty of Electrical Engineering, Czech Technical University in Prague, Czech Republic.

\*Corresponding author: filip.novak@fel.cvut.cz

This work was funded by CTU grant no SGS23/177/OHK3/3T/13, by the Czech Science Foundation (GAČR) under research project no. 23-06162M, and by the European Union under the project Robotics and advanced industrial production (reg. no. CZ.02.01.01/00/22.008/0004590).



Fig. 1. Long-exposure photo of drones carrying blue lights taken during a race flight at the A2RL Drone Racing Challenge 2025.

onboard sensors is strictly limited and no external localization system, e.g., a motion capture system, is available. Robust state estimation under such extreme conditions has become a main topic of interest for many research studies [4]–[9].

Human pilots have already shown the potential of agile lightweight UAVs during drone racing leagues, where they are able to control the UAV at high speeds, executing aggressive maneuvers through complex environments while avoiding obstacles and other drones. To enhance the capabilities and performance of autonomous UAVs and to reduce the gap between them and human pilots, the A2RL Drone Racing Challenge<sup>1</sup> was launched (see Fig. 1). The competition allowed each UAV to carry only a single RGB monocular camera, a flight controller with Inertial Measurement Unit (IMU), and a lightweight onboard computer. The goal was to fly through a predefined sequence of gates at maximum speed to minimize overall lap time, creating harsh and competitive conditions for testing high-speed autonomous flights. In competitions, many teams rely solely on end-to-end deep learning solutions, which perform well for racing. However, such methods are unsuitable for industrial or safety-critical applications, as they lack theoretical analysis and guarantees required for contingency planning. In contrast, our approach decomposes the problem into planning, state estimation, and an MPC control framework, where Lyapunov stability theory provides formal guarantees.

The state-of-the-art methods rely on more complex hardware, such as stereo cameras and rangefinders [6], or they depend on UAV states provided by Visual-Inertial Odometry (VIO) [6], [7], which fuses data from a single RGB camera and an IMU. However, VIO suffers from drifts, inaccuracies, and slow reaction to aggressive changes in all UAV states. The method presented in [6] uses uncorrected linear and angular velocities, which cause significant issues for the UAV

<sup>1</sup><https://a2rl.io/autonomous-drone-race>

controller. Similarly, the approach [7] relies on uncorrected attitude and angular rates, leading to problems for controller and onboard vision-based systems.

Our approach running at 100 Hz leverages VIO [10], but compared to the state-of-the-art methods [6], [7], we correct all UAV states, including position, orientation, linear velocity and angular velocity. We also use our onboard landmark-based camera measurement system, which uses known landmarks in an environment that are detectable in camera images, to provide an estimate of the UAV's position and orientation. However, any other method that provides such noisy partial UAV state estimates within the operating area can also be used.

In order to reduce VIO translational drift as well as attitude and velocity inaccuracies, our method fuses the estimated states obtained from detections of known landmarks with VIO and IMU data. We introduce a novel model of VIO drift that includes translation, linear velocity, yaw angle, and yaw rate, where the velocities are influenced by artificial friction to increase accuracy even when the onboard camera system temporarily stops providing usable data. Additionally, IMU data are directly fused into the attitude estimation in our pipeline, enabling higher accuracy and faster response to rapid maneuvers compared to state-of-the-art methods [6], [7]. We reduced orientation Root Mean Square Error (RMSE) by 70 %, linear velocity RMSE by 16 %, and angular velocity RMSE by factor of 8 compared to [7] and [6]. The presented estimation pipeline was also successfully deployed at the A2RL Drone Racing Challenge 2025<sup>1</sup>, where we reached the finals among the top four teams and won a medal, achieving top performance among decomposed classical approaches suitable for industrial and safety-critical applications.

## II. RELATED WORKS

Recent research has explored UAV state estimation using known landmarks for relative localization [5], [8]. These deep learning-based methods detect the next racing gate in camera image frames and guide the UAV towards its center. However, they fail if gates are not detected in the camera's Field of View (FOV). In practical scenarios, such as inspection and surveillance, the desired landmarks are not always visible in the camera images. Furthermore, these methods do not generalize well to tasks and environments beyond those on which they were trained. Several studies have adopted deep learning techniques for indoor state estimation using a monocular camera combined with an IMU [9], [11], [12]. These methods provide end-to-end 6 Degrees of Freedom (DOFs) UAV state estimation from image sequences fused with an IMU. However, these methods require large training datasets, are computationally intensive, and generalize poorly to unseen environments.

VIO represents the typical method for state estimation in GNSS-denied environments, running onboard autonomous robots equipped with a monocular camera and IMU [10], [13]. VIO estimates camera motion from image sequences, a process known as Visual Odometry (VO) method, which is categorized into direct and feature-based methods. Direct

methods [14], [15] optimize photometric error defined over raw pixel-level intensities. They handle low-texture environments but are sensitive to initialization and illumination changes. In contrast, feature-based VO methods [10], [16] detect visual features in images and track them across successive image frames. Feature-based methods are generally more robust to initialization and illumination changes but tend to be more affected by motion blur compared to direct methods.

The performance and accuracy of the VO approaches are enhanced by fusing IMU measurements, leading to VIO methods. IMUs typically provide data at a much higher frequency than cameras. Therefore, the integration of IMU significantly improves estimation of UAV's attitude and motion tracking in cases of losing visual features [10], [15], [16]. Despite these improvements, all aforementioned VIO methods still suffer from drift, where the estimated position, orientation, and linear and angular velocity gradually deviate from ground-truth values over time, especially during fast flights with high motion blur [4]. Furthermore, UAV attitude estimates may lack precision and often respond slowly to rapid changes in orientation.

Researchers have also investigated the use of event cameras in VIO systems [17]–[19]. Event cameras aim to address key limitations of standard cameras, such as fixed frame rates, low dynamic range, and motion blur, which pose significant challenges for VIO algorithms. Unlike standard cameras, event cameras offer low latency, high dynamic range, and are inherently immune to motion blur. However, event-based VIO methods are still in the early stages of development and continue to suffer from drift. Other approaches incorporate vehicle dynamics and external force estimation into VIO frameworks [20]–[22], improving state estimation performance, especially at high speeds, but issues related to drift and inaccurate velocity estimation persist.

The approach presented in [6] employs a VIO method fused with measurements from a vision-based gate detector and a downward-facing laser rangefinder to achieve accurate state estimation in GNSS-denied environments. Gate detections serve as features used to compensate VIO drift and align the UAV with its intended path. A Kalman filter estimates the translational and rotational misalignment between the VIO frame and the inertial frame. However, this approach cannot compensate for inaccuracies in the estimated VIO velocities, which may cause significant issues for controllers, particularly during high-speed aggressive maneuvers. Furthermore, the use of a laser rangefinder and stereo cameras for VIO simplifies the problem compared to our scenario, which relies on a single monocular camera.

The approach [7] fuses only VIO estimates with gate detections. The method uses a known race track layout to estimate the UAV position based on detected gates. The position estimates derived from gate measurements are used to correct VIO translational and linear velocity drift, which is modeled as a simple double integrator with zero input. However, this method strongly relies on attitude and angular rate estimates provided by VIO. During high-speed aggressive

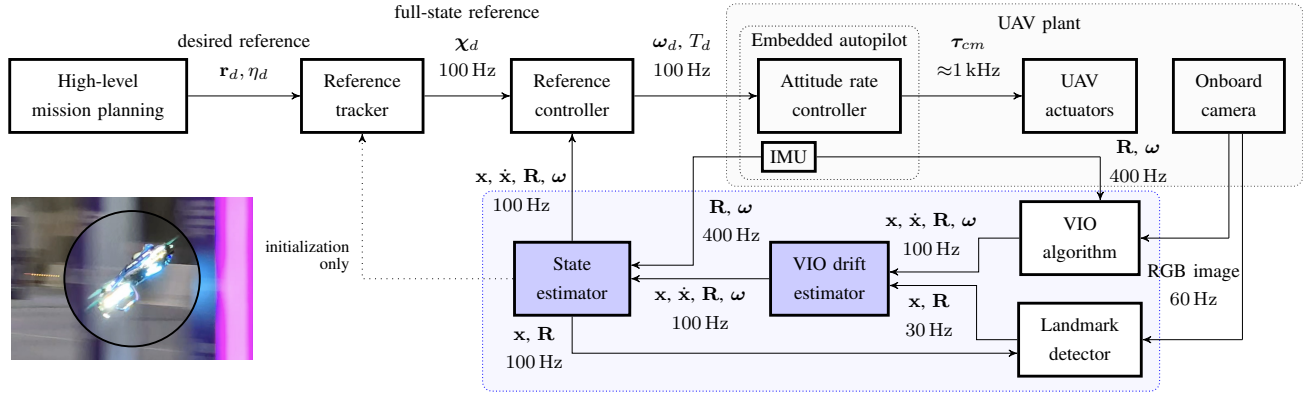


Fig. 2. This figure presents the pipeline diagram of the estimation approach proposed in this paper, highlighted by the light blue dotted rectangle and integrated into our drone racing framework. The *High-level mission planning* block provides the desired position and heading references  $(r_d, \eta_d)$  for the UAV to follow the race track. These references are passed to the *Reference tracker*, which generates a smooth and dynamically feasible reference  $\chi_d$  for the *Reference controller*. The *Reference controller* computes the desired thrust and angular velocities  $(\omega_d, T_d)$  for the embedded flight controller, which then sends actuator commands  $\tau_{cm}$  to the *UAV actuators*. The *VIO algorithm* uses *IMU* data and onboard camera images to estimate the UAV position  $\mathbf{x}$ , orientation  $\mathbf{R}$ , linear velocity  $\dot{\mathbf{x}}$ , and angular velocity  $\omega$ . The *VIO drift estimator* estimates the drift in the *VIO* states using position  $\mathbf{x}$  and orientation  $\mathbf{R}$  measurements from the *Landmark detector*. The *State estimator* fuses data from the *IMU*, *VIO drift estimator*, and *VIO algorithm* to estimate the UAV position, orientation, and linear and angular velocities  $(\mathbf{x}, \dot{\mathbf{x}}, \mathbf{R}, \omega)$ .

maneuvers, VIO estimates of attitude and angular rates are also subject to drift and latency. Such an inaccurate attitude estimates introduce significant errors in onboard camera-based measurement systems.

In contrast to the most relevant state-of-the-art methods [6], [7], our approach: (1) compensates for translational, rotational, and both linear and angular velocity drifts in the VIO state estimates, (2) introduces a novel drift model and directly fuses IMU data into the final UAV state estimate, enabling faster and more accurate responses to aggressive attitude changes, and (3) addresses the crucial issue of outliers arising in data from the onboard vision-based measurement system. The source code is available to the public as open-source (available upon publication). Our method is compatible with any direct or feature-based VIO method presented above, and it can integrate with arbitrary vision-based measurement systems.

### III. METHODOLOGY

The pipeline diagram of the proposed system is illustrated in Fig. 2. Our approach uses the VIO algorithm [10], which utilizes onboard IMU and RGB camera data. The VIO module provides drifting and inaccurate UAV state estimates to the VIO drift estimator, where the drift is compensated using additional data from our onboard landmark-based camera measurement system, i.e., Landmark detector, that provides estimated position and orientation of the UAV at 30 Hz based on detection of gates with known position. The corrected states from the VIO drift estimator are subsequently fused with the onboard high-rate IMU measurements (400 Hz) in the State estimator block (see Fig. 2), yielding full-state estimates that are provided to the Reference controller [23] at 100 Hz. The Reference controller tracks the desired full-state reference produced by the Reference tracker, which follows a trajectory precomputed using the minimum-time trajectory

generation method for the point-mass model [24]. Finally, the Reference controller transmits the control commands to the embedded autopilot, which actuates the UAV's motors accordingly.

In our approach, we estimate the full 6 DOF UAV state

$$\mathbf{x}_{\text{uav}} = (x, y, z, \phi, \theta, \psi, \dot{x}, \dot{y}, \dot{z}, p, q, r)^T, \quad (1)$$

where  $\mathbf{p}_{\text{uav}} = (x, y, z)^T$  denotes the position in the world frame  $\mathcal{W}$ ,  $\Theta_{\text{uav}} = (\phi, \theta, \psi)^T$  represents the orientation in the  $\mathcal{W}$  frame in terms of roll, pitch, and yaw angles,  $\mathbf{v}_{\text{uav}} = (\dot{x}, \dot{y}, \dot{z})^T$  is the linear velocity in the  $\mathcal{W}$  frame, and  $\omega_{\text{uav}} = (p, q, r)^T$  corresponds to the angular velocity in the UAV body frame  $\mathcal{B}_w = \{\mathbf{b}_{w,x}, \mathbf{b}_{w,y}, \mathbf{b}_{w,z}\}$ . The UAV's position and orientation from VIO algorithm  $\mathbf{r}_{\text{vio}}^v = (\mathbf{p}_{\text{vio}}^v, \Theta_{\text{vio}}^v)^T$  are provided in a local reference frame  $\mathcal{V}$  defined at the initialization point of the VIO method, as illustrated in Fig. 3. The VIO linear velocity  $\mathbf{v}_{\text{vio}}$  and angular velocity  $\omega_{\text{vio}}$  of the UAV are expressed in the UAV body frame  $\mathcal{B}_v = \{\mathbf{b}_{v,x}, \mathbf{b}_{v,y}, \mathbf{b}_{v,z}\}$ . The UAV states in the  $\mathcal{V}$  frame are transformed into the  $\mathcal{W}$  using a static transformation  $\mathbf{T}_{\mathcal{V}}^{\mathcal{W}}$ , which is constructed from the known initial UAV position and orientation  $\mathbf{r}_{\text{init}}^w$  in the  $\mathcal{W}$  frame

$$\mathbf{r}_{\text{vio}}^w = \mathbf{T}_{\mathcal{V}}^{\mathcal{W}}(\mathbf{r}_{\text{vio}}^v). \quad (2)$$

The ground-truth position and orientation of the UAV in the  $\mathcal{W}$  frame are denoted as  $\mathbf{r}_{\text{gt}}^w$ . The ground-truth linear and angular velocities are defined in the UAV body frame  $\mathcal{B}_w = \{\mathbf{b}_{w,x}, \mathbf{b}_{w,y}, \mathbf{b}_{w,z}\}$ . The position and orientation VIO drift  $\mathbf{r}_{\text{drift}}^w$  in the  $\mathcal{W}$  frame is defined by the difference between the VIO states  $\mathbf{r}_{\text{vio}}^w$  and the ground-truth states  $\mathbf{r}_{\text{gt}}^w$ . The position  $\mathbf{p}_{\text{id}}^w$  and orientation  $\Theta_{\text{id}}^w$  measured by the onboard landmark-based camera system are provided in the  $\mathcal{W}$  frame.

#### A. VIO algorithm

The VINS-Mono [10] VIO algorithm is used as the primary inaccurate and drifting source of UAV states. How-

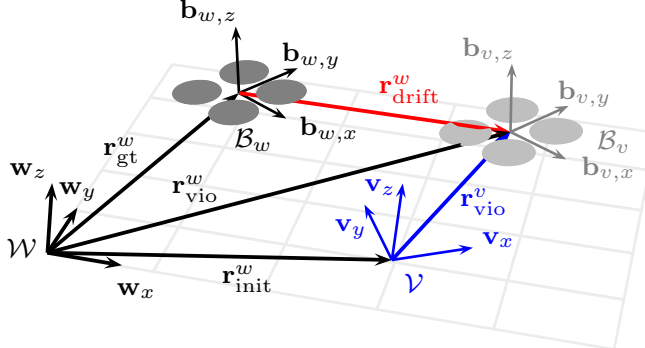


Fig. 3. The depiction of coordinate frames consisting of the world frame  $\mathcal{W}$ , UAV body frame  $\mathcal{B}_w$  expressed in the  $\mathcal{W}$  frame, VIO frame  $\mathcal{V}$ , and UAV body frame  $\mathcal{B}_v$  expressed in the  $\mathcal{V}$  frame. The relative position and orientation between the  $\mathcal{W}$  frame and the  $\mathcal{V}$  frame are represented by  $\mathbf{r}^w_{\text{init}}$ . The UAV position and orientation in  $\mathcal{W}$  frame are denoted as  $\mathbf{r}^w_{\text{gt}}$ . The UAV position and orientation estimated by the VIO algorithm are provided in the  $\mathcal{V}$  frame and denoted as  $\mathbf{r}^v_{\text{vio}}$ . The vector  $\mathbf{r}^v_{\text{vio}}$  represents the VIO-estimated UAV position and orientation expressed in the  $\mathcal{W}$  frame. The VIO drift is expressed as  $\mathbf{r}^w_{\text{drift}}$ .

ever, the proposed method is agnostic to the choice of VIO algorithm and was also successfully deployed with the OpenVINS VIO algorithm [16]. These VIO methods require only a single camera and an IMU to estimate the full 6 DOF robot state. The VINS-Mono algorithm [10] outputs the estimated states in the  $\mathcal{V}$  frame, which is established during initialization. The initialization procedure estimates key parameters, including metric scale, gravity direction, and gyroscope bias.

Although VINS-Mono estimates the gravity vector during initialization, inaccuracies in this process lead to noticeable errors in roll and pitch. These errors occur because the gravity direction is inferred from short-term motion and IMU preintegration, both of which are sensitive to sensor noise, bias instability, and insufficient motion excitation during initialization. Consequently, the estimated gravity vector may deviate from the true vertical, resulting in a tilt of the  $\mathcal{V}$  frame. To address this issue, we positioned the drone on a level starting podium after VIO initialization, and then performed a calibration procedure. This procedure corrects the initial source of drift in VIO odometry by resetting the UAV's position, roll, and pitch to zero, thereby effectively re-aligning the  $\mathcal{V}$  frame with the true gravity direction

$$\mathbf{p}_{\text{vio}}(t) = \mathbf{p}_{\text{vio},u}(t) - \mathbf{p}_{\text{vio},u}(t_{\text{init}}), \quad (3)$$

$$\mathbf{q}_{\text{vio}}(t) = \mathbf{q}_{\text{vio},u}^{-1}(t_{\text{init}}) \otimes \mathbf{q}_{\text{vio},u}(t), \quad (4)$$

where  $\mathbf{p}_{\text{vio}}(t)$  is the calibrated VIO position at time  $t$ ,  $\mathbf{p}_{\text{vio},u}(t)$  is the uncalibrated VIO position at time  $t$ ,  $\mathbf{p}_{\text{vio},u}(t_{\text{init}})$  is the uncalibrated VIO position at time  $t_{\text{init}}$  when the calibration procedure is invoked,  $\mathbf{q}_{\text{vio}}(t)$  is the calibrated VIO orientation of the UAV expressed as a quaternion,  $\mathbf{q}_{\text{vio},u}(t_{\text{init}})$  is the uncalibrated orientation quaternion at time  $t_{\text{init}}$ ,  $\otimes$  denotes the quaternion multiplication. By ensuring that the UAV starts from a known, level orientation, this procedure effectively removes accumulated attitude and position offsets, leading to more

accurate and stable state estimation during operation.

### B. Onboard landmark-based camera measurement system

To correct the drifting odometry from the VIO pipeline, we utilize an onboard landmark-based camera measurement system, referred to as Landmark detector (Fig. 2). The Landmark detector provides estimated UAV states in the  $\mathcal{W}$  frame using predefined static landmarks. In our scenario, we use racing gates as known static landmarks. The Landmark detector computes the UAV's position  $\mathbf{p}_{\text{ld}}^w$  and orientation  $\Theta_{\text{ld}}^w$  in the  $\mathcal{W}$  frame using a monocular RGB camera and the most recent estimated UAV states. The system operates in real time by combining deep learning-based corner detection, geometric reasoning, and nonlinear optimization to estimate the UAV states relative to known gate locations in the environment. Since the Landmark detector is not the primary focus or contribution of this paper, we provide only a brief description, as our proposed method uses its outputs for sensor fusion.

The Landmark detector processes RGB images from the UAV's onboard camera using a convolutional neural network based on the U-Net architecture [6]. The network adopts an encoder-decoder structure with skip connections, consisting of five convolutional blocks (32, 64, 128, 256, and 512 channels) for feature extraction and transposed convolutions for upsampling. Each block utilizes  $3 \times 3$  kernels with padding to preserve spatial dimensions. The final  $1 \times 1$  convolution layer outputs 12 feature maps: 4 heatmaps corresponding to corner keypoints and 8 maps representing two-dimensional vector fields that describe the 4 gate edges.

Detected corners and edges are first used to assemble gate candidates. These detected gate candidates are then matched to known real-world gate positions. Subsequently, the Landmark detector optimizes the UAV states  $\mathbf{p}_{\text{ld}}^w$  and  $\Theta_{\text{ld}}^w$  by minimizing the difference between optical rays projected from detected gate corners in the camera images and the corresponding real-world 3D positions of the gate corners. The optimization is initialized using the most recent estimated UAV position and orientation  $\mathbf{r}_{\text{uav}}^w$ . Since roll  $\phi_{\text{ld}}$  and pitch  $\theta_{\text{ld}}$  are highly unstable and noisy, we fuse more accurate IMU measurements and use only  $\mathbf{x}_{\text{ld}}^w = (x_{\text{ld}}, y_{\text{ld}}, z_{\text{ld}}, \psi_{\text{ld}})^\top$  from the Landmark detector. The reprojection error serves as the cost metric and is converted into a confidence score  $c_{\text{ld}}$  using a Gaussian weighting function

$$c_{\text{ld}} = \exp \left( -\frac{e_r^2}{2\sigma^2} \right) \left( 1 - \exp(-\beta N_p) \right), \quad (5)$$

where  $e_r$  is the reprojection error,  $\sigma$  is set to 0.15,  $\beta$  is 0.4, and  $N_p$  is the number of gate corners used in optimization to determine the UAV state. The estimated UAV state  $\mathbf{x}_{\text{ld}}^w$  and its associated confidence  $c_{\text{ld}}$  are then fused by our estimation pipeline as shown in Fig. 2.

### C. VIO drift estimation

We model the drift as a discrete linear system

$$\mathbf{x}_d(t + dt) = \mathbf{A}_d \mathbf{x}_d(t) + \mathbf{w}_{\text{noise}}(t), \quad (6)$$

where  $t$  is the current time, the drift state  $\mathbf{x}_d$  consists of the translational drift  $\mathbf{p}_d = (x_d, y_d, z_d)^\top$  with corresponding drift velocities  $\mathbf{v}_d = (\dot{x}_d, \dot{y}_d, \dot{z}_d)^\top$ , as well as the yaw drift  $\psi_d$  with its corresponding drift rate  $r_d$

$$\mathbf{x}_d = (x_d \ \dot{x}_d \ y_d \ \dot{y}_d \ z_d \ \dot{z}_d \ \psi_d \ r_d)^\top, \quad (7)$$

$$\mathbf{A}_d = \begin{pmatrix} 1 & dt & 0 & 0 & 0 & 0 & 0 & 0 \\ 0 & 1 - f_x & 0 & 0 & 0 & 0 & 0 & 0 \\ 0 & 0 & 1 & dt & 0 & 0 & 0 & 0 \\ 0 & 0 & 0 & 1 - f_y & 0 & 0 & 0 & 0 \\ 0 & 0 & 0 & 0 & 1 & dt & 0 & 0 \\ 0 & 0 & 0 & 0 & 0 & 1 - f_z & 0 & 0 \\ 0 & 0 & 0 & 0 & 0 & 0 & 1 & dt \\ 0 & 0 & 0 & 0 & 0 & 0 & 0 & 1 - f_\psi \end{pmatrix}. \quad (8)$$

The parameter  $dt$  represents the discrete time update step. Each drift velocity component  $(\dot{x}_d, \dot{y}_d, \dot{z}_d)$  and yaw drift rate  $r_d$  is influenced by the corresponding friction parameter  $f_x, f_y, f_z, f_\psi$ , which limit the rate of drift change. Since the VIO drift cannot be directly affected or corrected through known control inputs, the model does not include any control input term. However, in our drift model, we incorporate an unknown input vector  $\mathbf{w}_{\text{noise}} \in \mathbb{R}^8$  to account for unmodeled dynamics, disturbances, and uncertainties. Each component of  $\mathbf{w}_{\text{noise}}$  is modeled as independent zero-mean Gaussian noise with covariance values  $Q_{x_d}, Q_{y_d}, Q_{z_d}, Q_{\psi_d}, Q_{\dot{x}_d}, Q_{\dot{y}_d}, Q_{\dot{z}_d}, Q_{r_d} \in \mathbb{R}^+$  corresponding to the individual drift states.

The VIO drift cannot be directly measured or observed. To estimate VIO drift, we utilize the Landmark detector (Sec. III-B) that provides a noisy estimate of the UAV state  $\mathbf{x}_{\text{ld}}^w$  in the  $\mathcal{W}$  frame. The position and yaw drift measurement  $\mathbf{z}$  is then computed as the difference between the VIO position and yaw  $(x_{\text{vio}}, y_{\text{vio}}, z_{\text{vio}}, \psi_{\text{vio}})$  expressed in  $\mathcal{W}$  frame (2) and the camera-based estimate  $\mathbf{x}_{\text{ld}}^w$

$$\mathbf{z} = (x_{\text{vio}}, y_{\text{vio}}, z_{\text{vio}}, \psi_{\text{vio}})^\top - (x_{\text{ld}}, y_{\text{ld}}, z_{\text{ld}}, \psi_{\text{ld}})^\top. \quad (9)$$

The onboard camera measurement system typically operates at a slower rate than VIO. In our case, VIO runs at 100 Hz and the Landmark detector runs at 30 Hz. To align these states in time, we store the last 1 s of incoming VIO odometry in a buffer and select the sample with the timestamp closest to that of the camera measurement.

The measurement equation defines how the system states are observed through available measurements. The model  $\mathbf{z}_d$  for our measurements  $\mathbf{z}$  at time  $t$  is given by

$$\mathbf{z}_d(t) = \mathbf{H}_d \mathbf{x}_d(t) + \mathbf{v}_{\text{noise}}(t), \quad (10)$$

$$\mathbf{H}_d = \begin{pmatrix} 1 & 0 & 0 & 0 & 0 & 0 & 0 & 0 \\ 0 & 0 & 1 & 0 & 0 & 0 & 0 & 0 \\ 0 & 0 & 0 & 0 & 1 & 0 & 0 & 0 \\ 0 & 0 & 0 & 0 & 0 & 0 & 1 & 0 \end{pmatrix}, \quad (11)$$

where the vector  $\mathbf{v}_{\text{noise}}$  represents measurement noise introduced by sensing uncertainties and errors. Similar to  $\mathbf{w}_{\text{noise}}$ , each component of  $\mathbf{v}_{\text{noise}}$  is modeled as independent Gaussian noise with zero mean and covariance values  $R_{x_d}, R_{y_d}, R_{z_d}, R_{\psi_d} \in \mathbb{R}^+$ .

We use a Linear Kalman Filter (LKF) as a state estimator for VIO drift. The LKF consists of two steps: 1) the prediction step and 2) the correction step. In the prediction step, the system model is used to propagate the current state estimate and the corresponding covariance matrix  $\mathbf{P}_d$  of the state  $\mathbf{x}_d$  forward in time

$$\mathbf{x}_d(t + dt) = \mathbf{A}_d \mathbf{x}_d(t), \quad (12)$$

$$\mathbf{P}_d(t + dt) = \mathbf{A}_d \mathbf{P}_d(t) \mathbf{A}_d^\top + \mathbf{Q}_d, \quad (13)$$

where the covariance matrix  $\mathbf{Q}_d$  is a diagonal matrix

$$\mathbf{Q}_d = \text{diag}\{Q_{x_d}, Q_{y_d}, Q_{z_d}, Q_{\psi_d}, Q_{\dot{x}_d}, Q_{\dot{y}_d}, Q_{\dot{z}_d}, Q_{r_d}\}. \quad (14)$$

The prediction step runs at 100 Hz, resulting in  $dt = 0.01$  s. In the correction step, the current estimated state is updated using the incoming measurement  $\mathbf{z}(t)$

$$\mathbf{G}_d(t) := \mathbf{P}_d(t) \mathbf{H}_d(t)^\top (\mathbf{H}_d \mathbf{P}_d(t) \mathbf{H}_d^\top + \mathbf{R}_d)^{-1}, \quad (15)$$

$$\mathbf{x}_d(t) := \mathbf{x}_d(t) + \mathbf{G}_d(t) (\mathbf{z}(t) - \mathbf{H}_d \mathbf{x}_d(t)), \quad (16)$$

$$\mathbf{P}_d(t) := \mathbf{P}_d(t) - \mathbf{G}_d(t) \mathbf{H}_d \mathbf{P}_d(t), \quad (17)$$

where  $\mathbf{R}_d$  is defined as a diagonal matrix

$$\mathbf{R}_d = \text{diag}\{R_{x_d}, R_{y_d}, R_{z_d}, R_{\psi_d}\}. \quad (18)$$

The covariances  $R_{x_d}, R_{y_d}, R_{z_d}$ , and  $R_{\psi_d}$  are estimated using the confidence  $c_{\text{ld}}$  of the Landmark detector (5) as follows

$$R_{\{x_d, y_d, z_d, \psi_d\}} = \frac{a_{rv}}{1 + \exp(-b_{rv}(c_{\text{ld}} - c_{rv}))} + d_{rv}, \quad (19)$$

where  $a_{rv}, b_{rv}, c_{rv}$ , and  $d_{rv}$  are parameters in  $\mathbb{R}^+$ . Since the LKF is highly sensitive to outliers, we reject measurements deemed unreliable based on the confidence  $c_{\text{ld}}$  defined in (5). If the measurement confidence  $c_{\text{ld}}$  falls below a predefined threshold  $t_{c_{\text{ld}}} = 0.5$ , the measurement is not fused.

#### D. State estimator

All data from the VIO algorithm, the estimated VIO drift, and the IMU measurements are fused in the State estimator (see Fig. 2). The corrected UAV position  $\mathbf{p}_{\text{uav}}$  is computed as the difference between the VIO position transformed into the  $\mathcal{W}$  frame  $\mathbf{p}_{\text{vio}}^w$  and the estimated position drift  $\mathbf{p}_d$  as

$$\mathbf{p}_{\text{uav}}(t) = \mathbf{p}_{\text{vio}}^w(t) - \mathbf{p}_d(t). \quad (20)$$

The roll  $\phi_{\text{vio}}$  and pitch  $\theta_{\text{vio}}$  obtained from the VIO algorithm are inaccurate and delayed due to z-axis alignment issues and the lack of incorporation into the graph optimization [10]. Therefore, the roll angle  $\phi_{\text{imu}}$  and pitch angle  $\theta_{\text{imu}}$  are taken from the IMU data, which are filtered using a low-pass filter and a dynamic notch filter to ensure fast and accurate response during aggressive maneuvers in agile flights. The yaw angle is taken from the VIO algorithm, as it is optimized through global pose graph optimization, which makes it more accurate compared to the yaw  $\psi_{\text{imu}}$  derived from the IMU. To further reduce yaw drift, the estimated yaw drift  $\psi_d$  is subtracted from the VIO yaw angle  $\psi_{\text{vio}}$  in  $\mathcal{W}$  frame

$$\psi_{\text{uav}}(t) = \psi_{\text{vio}}(t) - \psi_d(t). \quad (21)$$

The linear velocities are taken from the VIO algorithm and corrected using the estimated drift velocities. We assume that the velocity reported by the VIO algorithm corresponds to the derivative of the VIO position. The linear velocity from the VIO algorithm is expressed in the  $\mathcal{B}_v$  frame, whereas the drift linear velocity is estimated in the  $\mathcal{W}$  frame. Therefore, the VIO velocities are transformed from the  $\mathcal{B}_v$  frame to the  $\mathcal{W}$  frame using the rotation matrix  $\mathbf{R}_{\mathcal{B}_v}^{\mathcal{W}}$

$$\mathbf{v}_{\text{vio}}^w(t) = \mathbf{R}_{\mathcal{B}_v}^{\mathcal{W}} \mathbf{v}_{\text{vio}}^{\mathcal{B}_v}(t), \quad (22)$$

$$\mathbf{v}_{\text{uav}}(t) = \mathbf{v}_{\text{vio}}^w(t) - \mathbf{v}_d(t). \quad (23)$$

The roll rate  $p_{\text{imu}}$  and pitch rate  $q_{\text{imu}}$  are taken directly from the IMU. However, the yaw rate  $r_{\text{vio}}$  from the VIO algorithm is corrected using the estimated drift rate  $r_d$

$$r_{\text{uav}} = r_{\text{vio}} - r_d. \quad (24)$$

To summarize, the corrected UAV position  $\mathbf{p}_{\text{uav}}$ , orientation  $\Theta_{\text{uav}}$ , linear velocity  $\mathbf{v}_{\text{uav}}$ , and angular velocity  $\omega_{\text{uav}}$  are computed as follows

$$\mathbf{p}_{\text{uav}}(t) = \mathbf{p}_{\text{vio}}^w(t) - \mathbf{p}_d(t), \quad (25)$$

$$\Theta_{\text{uav}}(t) = (\phi_{\text{imu}}(t), \theta_{\text{imu}}(t), \psi_{\text{vio}}(t) - \psi_d(t))^T, \quad (26)$$

$$\mathbf{v}_{\text{uav}}(t) = \mathbf{v}_{\text{vio}}^w(t) - \mathbf{v}_d(t), \quad (27)$$

$$\omega_{\text{uav}}(t) = (p_{\text{imu}}(t), q_{\text{imu}}(t), r_{\text{vio}}(t) - r_d(t))^T. \quad (28)$$

This estimation pipeline enables fast flights through gates in drone racing, providing accurate UAV states even during aggressive maneuvers. Our method uses VIO odometry, which does not require predefined landmarks and is subsequently corrected using the estimated drift states. During fast and aggressive flights, the drift changes dynamically, and our estimation approach captures these variations through the drift velocity estimation. Due to the drift velocity estimation, our approach maintains accurate state estimation even when the Landmark detector temporarily cannot provide measurements, for example, when landmarks are not visible in the camera frame, or they are too distant from the camera, which negatively influences the precision of the onboard camera measurement system. The direct fusion of IMU data enables fast and accurate estimation of roll, pitch, and their corresponding rates during aggressive maneuvers.

## IV. RESULTS

The proposed method was first evaluated in Gazebo simulations and subsequently tested in real-world experiments and a racing competition<sup>1</sup>. The gates are square-shaped, with an inner opening of 1.5 m and an outer dimension of 2.7 m. The UAV, including its propellers, fits within a bounding box of dimensions  $0.4 \times 0.4 \times 0.25$  m.

### A. Gazebo simulations

We ran 1600 simulations to evaluate the robustness of our approach with respect to delay  $\tau_d$  and noise in the Landmark detector. The noise was modeled as Gaussian with zero mean and standard deviation equal to  $\sigma_{\text{p}_{\text{ld}}}^2$  for the position noise and  $\sigma_{\psi_{\text{ld}}}^2$  for the yaw noise. For each combination of  $\tau_d = \{0, 15, 30, 60\}$  ms with  $\sigma_{\text{p}_{\text{ld}}}^2 = \{0.001, 0.01, 0.1, 1.0\}$  m

TABLE I  
RMSE RESULTS FROM THE SIMULATIONS.

$\sigma_{\text{p}_{\text{ld}}}^2$ [m]	0.001	0.01	0.1	1.0	0.001	0.01	0.1	1.0					
$\sigma_{\psi_{\text{ld}}}^2$ [rad]	0.001	0.01	0.1	1.0	0.001	0.01	0.1	1.0					
$\tau_d$ [ms]	State				Our approach				VIO				
0	$\mathbf{p}$ [m]	0.35	0.40	0.45	1.11	6.39	7.55	8.68	8.44	0.23	0.23	0.26	0.29
	$\Theta$ [rad]	0.04	0.04	0.09	0.57	1.27	1.30	1.49	1.57	0.09	0.23	0.14	0.32
	$\mathbf{v}$ [ $\text{m s}^{-1}$ ]	0.96	1.00	1.09	1.40	1.13	1.15	1.11	1.09	0.76	1.52	0.98	1.68
	$\omega$ [ $\text{rad s}^{-1}$ ]	0.24	0.23	0.24	0.24	1.21	1.14	1.18	1.09	0.55	0.48	0.59	0.88
15	$\mathbf{p}$ [m]	0.23	0.47	0.32	1.19	3.94	8.77	5.63	9.39	0.04	0.04	0.09	0.57
	$\Theta$ [rad]	0.04	0.04	0.09	0.57	0.09	0.23	0.14	0.32	1.01	0.92	0.94	1.08
	$\mathbf{v}$ [ $\text{m s}^{-1}$ ]	0.69	1.08	0.81	1.49	1.34	1.26	1.46	0.84	0.24	0.23	0.24	0.24
	$\omega$ [ $\text{rad s}^{-1}$ ]	0.23	0.23	0.24	0.23	1.14	1.15	1.10	1.20	0.72	0.66	0.73	1.09
30	$\mathbf{p}$ [m]	0.55	0.48	0.59	0.88	6.96	7.62	7.64	4.17	0.04	0.04	0.10	0.56
	$\Theta$ [rad]	0.04	0.04	0.10	0.56	0.25	0.18	0.28	0.10	1.01	0.92	0.94	1.08
	$\mathbf{v}$ [ $\text{m s}^{-1}$ ]	1.01	0.92	0.94	1.08	1.40	1.26	1.46	0.84	0.24	0.23	0.24	0.24
	$\omega$ [ $\text{rad s}^{-1}$ ]	0.24	0.23	0.24	0.24	1.14	1.15	1.10	1.20	0.72	0.66	0.73	1.09
60	$\mathbf{p}$ [m]	0.05	0.05	0.10	0.56	0.25	0.21	0.23	0.18	1.06	0.97	1.06	1.13
	$\Theta$ [rad]	0.05	0.05	0.10	0.56	1.40	1.26	1.40	1.19	0.24	0.23	0.23	0.24
	$\mathbf{v}$ [ $\text{m s}^{-1}$ ]	1.06	0.97	1.06	1.13	1.14	1.15	1.14	1.16	0.72	0.66	0.73	1.09
	$\omega$ [ $\text{rad s}^{-1}$ ]	0.24	0.23	0.23	0.24	1.14	1.15	1.14	1.16	0.55	0.48	0.59	0.88

and  $\sigma_{\psi_{\text{ld}}}^2 = \{0.001, 0.01, 0.1, 1.0\}$  rad, we conducted 100 simulations and computed the mean RMSE for individual UAV states for both our approach and VIO, relative to the ground-truth values. The results are summarized in Tab. I and show that our system operates effectively even in the presence of delays and noise in the Landmark detector. A significant increase in RMSE occurs for all states when  $\sigma_{\text{p}_{\text{ld}}}^2$  and  $\sigma_{\psi_{\text{ld}}}^2$  reach 1.0. At this level, the linear velocity estimates from our approach and VIO exhibit similar precision. In all other cases, our approach outperforms the VIO method across all states. Consequently, our method also surpasses [6], where VIO velocities remain uncorrected, and [7], which directly uses attitude and angular rates from VIO.

### B. Real-world experiments

To evaluate the proposed method against ground-truth data, we conducted real-world experiments on an outdoor race track (see Fig. 4) consisting of 5 gates, as illustrated in Fig. 5. The fourth gate was designed as a double gate, where the UAV performed a Split-S maneuver from the top to the bottom gate. Ground-truth data were obtained using a Global Positioning System (GPS)-Real-time Kinematics (RTK) system. The UAV was equipped with a Holybro Pixhawk 6C Mini flight controller and a Holybro H-RTK F9P Helical GPS-RTK module.

In each of our flight tests, we performed 2 laps on the track, running both our proposed estimation approach and the RTK-based state estimator simultaneously for comparison. During these experiments, the UAV reached speeds of up to  $10 \text{ m s}^{-1}$ . Figure 5 presents a 2D plot of the track in the  $x$ - $y$  plane, showing the gate positions, podium position, RTK states, results of our approach (Sec. III-D), VIO states (Sec. III-A), and outputs from the Landmark detector (Sec. III-B). As illustrated, the VIO estimates (shown in green) began drifting shortly after the start of the trajectory. The measurements from the Landmark detector are highly noisy and exhibit significant spikes. In contrast, the states estimated by our approach follow the RTK ground-truth data throughout the flight.



Fig. 4. Custom-built outdoor track used to verify our approach.

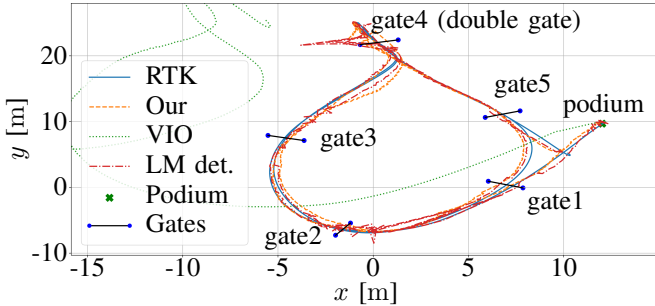


Fig. 5. Top view of the outdoor track showing the RTK states, results of our approach, VIO states, and data from the Landmark detector (LM det.).

The RMSE values for individual UAV states from our flights are summarized in Tab. II. Since the Landmark detector provides only position and orientation measurements, RMSE for linear and angular velocities is not reported. Our proposed method achieved the lowest RMSE values across all individual UAV states (see Tab. II). Table III shows the RMSE, mean error, maximum error, and standard deviation of the error for position  $\mathbf{p}$ , orientation  $\Theta$ , linear velocity  $\mathbf{v}$ , and angular velocity  $\omega$ . The results confirm that VIO alone is insufficient to complete the race track due to accumulated drift. The position RMSE of the VIO is reduced by a factor of 27 using our approach (Tab. III).

Because the approach in [7] directly uses orientation  $\Theta$  and angular velocity  $\omega$  from VIO, our approach reduces RMSE of  $\Theta$  by 70 % and RMSE of  $\omega$  by a factor of 8 compared to [7] (see Tab. III). Moreover, the RMSE of linear velocity  $\mathbf{v}$  is reduced by 16 % and RMSE of angular velocity  $\omega$  is reduced by a factor of 8 relative to [6], which directly uses  $\mathbf{v}$  and  $\omega$  from VIO (see Tab. III). The mean error across all states further support this comparison (see Tab. III). Additionally, our approach achieves the lowest standard deviation and the lowest maximum error for all states compared to other methods.

### C. A2RL Drone Racing Challenge

The UAV used during A2RL Drone Racing Challenge<sup>1</sup> was equipped with an 8 MP camera, an onboard computer, and a flight controller with an IMU. The track consisted of 10 gates, with 1 double gate in which split-S maneuver was required. The teams had to fly 2 laps through gates. The team with the shortest time won, and the time was measured from passing the first gate to passing the last gate in the second

TABLE II  
RMSE OF INDIVIDUAL UAV STATES RELATIVE TO GROUND-TRUTH  
VALUES IN THE REAL-WORLD EXPERIMENT.

Method	Position [m]			Orientation [rad]		
	$x$	$y$	$z$	roll $\phi$	pitch $\theta$	yaw $\psi$
Our approach	<b>0.374</b>	<b>0.493</b>	<b>0.193</b>	<b>0.012</b>	<b>0.016</b>	<b>0.083</b>
VIO	12.325	11.823	3.532	0.038	0.040	0.275
Landmark detector	0.541	0.554	0.221	0.056	0.049	0.115
Linear velocity [ $\text{m s}^{-1}$ ]			Angular velocity [ $\text{rad s}^{-1}$ ]			
Our approach	$\dot{x}$	$\dot{y}$	$\dot{z}$	$p$	$q$	$r$
	<b>0.568</b>	<b>1.184</b>	<b>0.398</b>	<b>0.090</b>	<b>0.078</b>	<b>0.024</b>
VIO	0.766	1.376	0.465	0.626	0.738	0.278

TABLE III  
RMSE, MEAN ERROR, STANDARD DEVIATION OF THE ERROR, AND  
MAXIMUM ERROR OF ESTIMATED UAV STATES USING OUR APPROACH  
COMPARED TO STATE-OF-THE-ART, VIO, AND LANDMARK DETECTOR.

Method	State	RMSE	Mean	Std. Dev.	Max
Our approach	$\mathbf{p}$ [m]	0.648	0.581	0.288	1.879
	$\Theta$ [rad]	0.085	0.064	0.056	0.268
	$\mathbf{v}$ [ $\text{m s}^{-1}$ ]	1.372	1.152	0.746	3.612
	$\omega$ [ $\text{rad s}^{-1}$ ]	0.121	0.079	0.092	0.759
VIO	$\mathbf{p}$ [m]	17.440	16.274	6.270	26.017
	$\Theta$ [rad]	0.281	0.277	0.047	0.414
	$\mathbf{v}$ [ $\text{m s}^{-1}$ ]	1.642	1.329	0.963	4.491
	$\omega$ [ $\text{rad s}^{-1}$ ]	1.007	0.803	0.607	3.389
Landmark detector	$\mathbf{p}$ [m]	0.805	0.612	0.523	7.584
	$\Theta$ [rad]	0.137	0.104	0.089	2.555

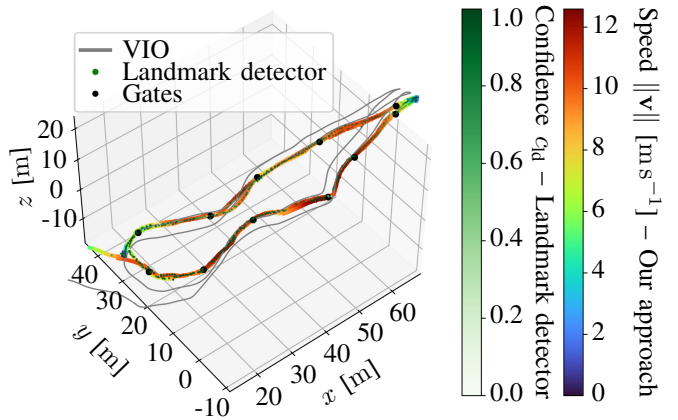


Fig. 6. 3D plot of the estimated UAV position using our approach, with color indicating the UAV speed. The VIO position is shown in grey. Measurements from the Landmark detector are represented as circles, with green color indicating confidence, and the race gates are shown as black circles.

lap. The part of the track is shown in Fig. 1, and the UAV flying on it is depicted in Fig. 2. In each round, the team had a 15-minute time window to perform as many flights as desired, with the fastest time recorded for the leaderboard of that round.

We completed 2 laps multiple times at speeds ranging from  $5 \text{ m s}^{-1}$  to  $12.5 \text{ m s}^{-1}$ . An example of our fastest trajectory is shown in Fig. 6, which clearly demonstrates that the VIO algorithm alone is insufficient for drone racing. Figure 7 shows the estimated individual UAV states  $\mathbf{x}_{\text{uav}}$  obtained using our approach. Using the presented estimation approach, our team successfully advanced through the qualification, quarterfinal, and semifinal rounds, reaching the finals alongside three other teams out of a total of 210 and winning a medal.

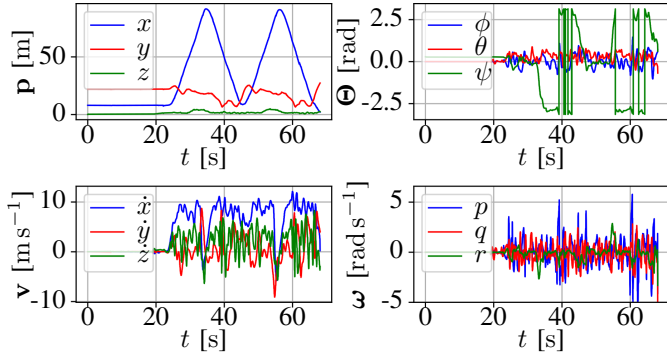


Fig. 7. Estimated UAV states during the A2RL finals using our approach.

## V. CONCLUSION

In this paper, we presented an approach for GNSS-denied UAV state estimation during fast vision-based flights and aggressive maneuvers in cluttered environments. Our method estimates UAV states in 6 DOFs (position, orientation, linear velocity, and angular velocity) using only a single RGB monocular camera, an IMU, and an onboard computer. It builds upon a VIO method that provides drifting and inaccurate states, which are corrected using measurements from the onboard landmark-based camera system. Our approach fuses data from VIO, the onboard landmark-based camera measurement system, and the IMU to estimate and compensate for VIO drift, correcting the UAV's position, orientation, and linear and angular velocities. For sensor fusion, we introduced a novel mathematical model of the drift. Additionally, directly incorporating IMU data into the final estimate ensures fast response and high precision even during highly aggressive maneuvers. Unlike end-to-end solutions, our method is well-suited for industrial and safety-critical applications, as it decomposes the problem into planning, state estimation, and control, where theoretical guarantees exist. The approach was extensively evaluated in simulations and real-world experiments, outperforming current state-of-the-art methods. Finally, we applied the proposed approach during the A2RL Drone Racing Challenge 2025<sup>1</sup>, where our team reached the final four out of 210 teams.

## REFERENCES

- [1] G. Silano, T. Baca, R. Penicka, D. Liuzza, and M. Saska, "Power line inspection tasks with multi-aerial robot systems via signal temporal logic specifications," *IEEE Robotics and Automation Letters*, vol. 6, no. 2, pp. 4169–4176, 2021.
- [2] R. R. Murphy, E. Steimle, C. Griffin, C. Collins, M. Hall, and K. Pratt, "Cooperative use of unmanned sea surface and micro aerial vehicles at Hurricane Wilma," *Journal of Field Robotics*, vol. 25, no. 3, pp. 164–180, 2008.
- [3] F. Nekovář, J. Faigl, and M. Saska, "Multi-vehicle dynamic water surface monitoring," *IEEE Robotics and Automation Letters*, vol. 8, no. 10, pp. 6323–6330, 2023.
- [4] J. Delméraco, T. Cieslewski, H. Rebecq, M. Faessler, and D. Scaramuzza, "Are We Ready for Autonomous Drone Racing? The UZH-FPV Drone Racing Dataset," in *2019 International Conference on Robotics and Automation (ICRA)*, May 2019, pp. 6713–6719.
- [5] E. Kaufmann, M. Gehrig, P. Foehn, R. Ranftl, A. Dosovitskiy, V. Koltun, and D. Scaramuzza, "Beauty and the Beast: Optimal Methods Meet Learning for Drone Racing," in *2019 International Conference on Robotics and Automation (ICRA)*, May 2019, pp. 690–696.
- [6] P. Foehn, D. Brescianini, E. Kaufmann, T. Cieslewski, M. Gehrig, M. Muglikar, and D. Scaramuzza, "AlphaPilot: Autonomous drone racing," *Autonomous Robots*, vol. 46, no. 1, pp. 307–320, Jan. 2022.
- [7] E. Kaufmann, L. Bauersfeld, A. Loquercio, M. Müller, V. Koltun, and D. Scaramuzza, "Champion-level drone racing using deep reinforcement learning," *Nature*, vol. 620, no. 7976, pp. 982–987, Aug. 2023.
- [8] S. Jung, S. Hwang, H. Shin, and D. H. Shim, "Perception, Guidance, and Navigation for Indoor Autonomous Drone Racing Using Deep Learning," *IEEE Robotics and Automation Letters*, vol. 3, no. 3, pp. 2539–2544, July 2018.
- [9] Y. Xu and G. C. H. E. de Croon, "CNN-based Ego-Motion Estimation for Fast MAV Maneuvers," in *2021 IEEE International Conference on Robotics and Automation (ICRA)*, May 2021, pp. 7606–7612.
- [10] T. Qin, P. Li, and S. Shen, "VINS-Mono: A Robust and Versatile Monocular Visual-Inertial State Estimator," *IEEE Transactions on Robotics*, vol. 34, no. 4, pp. 1004–1020, Aug. 2018.
- [11] W. Wang, Y. Hu, and S. Scherer, "TartanVO: A Generalizable Learning-based VO," in *Proceedings of the 2020 Conference on Robot Learning*. PMLR, Oct. 2021, pp. 1761–1772.
- [12] Y. Xu and G. C. De Croon, "CUAHN-VIO: Content-and-uncertainty-aware homography network for visual-inertial odometry," *Robotics and Autonomous Systems*, vol. 185, p. 104866, Mar. 2025.
- [13] D. Scaramuzza and Z. Zhang, "Aerial Robots, Visual-Inertial Odometry of," in *Encyclopedia of Robotics*. Springer, Berlin, Heidelberg, 2020, pp. 1–9.
- [14] J. Engel, V. Koltun, and D. Cremers, "Direct Sparse Odometry," *IEEE Transactions on Pattern Analysis and Machine Intelligence*, vol. 40, no. 3, pp. 611–625, Mar. 2018.
- [15] V. Usenko, J. Engel, J. Stückler, and D. Cremers, "Direct visual-inertial odometry with stereo cameras," in *2016 IEEE International Conference on Robotics and Automation (ICRA)*, May 2016, pp. 1885–1892.
- [16] P. Geneva, K. Eckenhoff, W. Lee, Y. Yang, and G. Huang, "OpenVINS: A Research Platform for Visual-Inertial Estimation," in *2020 IEEE International Conference on Robotics and Automation (ICRA)*, May 2020, pp. 4666–4672.
- [17] A. R. Vidal, H. Rebecq, T. Horstschaefer, and D. Scaramuzza, "Ultimate SLAM? Combining Events, Images, and IMU for Robust Visual SLAM in HDR and High-Speed Scenarios," *IEEE Robotics and Automation Letters*, vol. 3, no. 2, pp. 994–1001, Apr. 2018.
- [18] P. Chen, W. Guan, and P. Lu, "ESVIO: Event-Based Stereo Visual Inertial Odometry," *IEEE Robotics and Automation Letters*, vol. 8, no. 6, pp. 3661–3668, June 2023.
- [19] W. Guan, P. Chen, Y. Xie, and P. Lu, "PL-EVIO: Robust Monocular Event-Based Visual Inertial Odometry With Point and Line Features," *IEEE Transactions on Automation Science and Engineering*, vol. 21, no. 4, pp. 6277–6293, Oct. 2024.
- [20] B. Nisar, P. Foehn, D. Falanga, and D. Scaramuzza, "VIMO: Simultaneous Visual Inertial Model-Based Odometry and Force Estimation," *IEEE Robotics and Automation Letters*, vol. 4, no. 3, pp. 2785–2792, July 2019.
- [21] Z. Ding, T. Yang, K. Zhang, C. Xu, and F. Gao, "VID-Fusion: Robust Visual-Inertial-Dynamics Odometry for Accurate External Force Estimation," in *2021 IEEE International Conference on Robotics and Automation (ICRA)*, May 2021, pp. 14469–14475.
- [22] G. Cioffi, L. Bauersfeld, and D. Scaramuzza, "HDVIO: Improving Localization and Disturbance Estimation with Hybrid Dynamics VIO," in *Robotics: Science and Systems XIX*. Robotics: Science and Systems Foundation, July 2023.
- [23] P. M. Gupta, O. Procházka, J. Hřebec, M. Novosad, R. Pěnička, and M. Saska, "Lol-nmpc: Low-level dynamics integration in nonlinear model predictive control for unmanned aerial vehicles," in *2025 IEEE/RSJ International Conference on Intelligent Robots and Systems (IROS)*, 2025, pp. 1186–1193.
- [24] K. Teissing, M. Novosad, R. Penicka, and M. Saska, "Real-time planning of minimum-time trajectories for agile uav flight," *IEEE Robotics and Automation Letters*, vol. 9, no. 11, pp. 10351–10358, 2024.